A bionic multichannel nanofiber conduit carrying Tubastatin A for repairing injured spinal cord

Shiyang Liao [a,1], Yonghang Liu [b,1], Yanlong Kong [a,1], Haitao Shi [c], Bitong Xu [c], Bo Tang [c], Congbin Li [a], Yitian Chen [c], Jing Chen [d], Juan Du [b,**], Yadong Zhang [a,c,*]

[a] Fengxian Hospital, School of Medicine, Anhui University of Science and Technology, 6600 Nanfeng Hwy, Shanghai, 201499, PR China
[b] School of Chemistry and Chemical Engineering, Shanghai Engineering Research Center of Pharmaceutical Intelligent Equipment, Shanghai Frontiers Science Research Center for Druggability of Cardiovascular Non-coding RNA, Institute for Frontier Medical Technology, Shanghai University of Engineering Science, 333 Longteng Rd, Shanghai, 201620, PR China
[c] Department of Spine, Center for Orthopaedic Surgery, The Third Affiliated Hospital of Southern Medical University, 183 West Zhongshan Avenue, Guangzhou, 510515, PR China
[d] Shuguang Hospital Affiliated to Shanghai University of Traditional Chinese Medicine, 528 Zhangheng Rd, Shanghai, 201203, PR China

ARTICLE INFO

ABSTRACT

Spinal cord injury is a kind of nerve injury disease with high disability rate. The bioscaffold, which presents a biomimetic structure, can be used as "bridge" to fill the cavity formed by the liquefaction and necrosis of spinal nerve cells, and connects the two ends of the fracture to promote the effective recovery of nerve function. Tubasatin A (TUBA) is a potent selective histone deacetylase 6 (HDAC6) inhibitor, which can inhibit the over-expression of HDAC6 after spinal cord injury. However, TUBA is limited by high efflux ratios, low brain penetration and uptake in the treatment of spinal cord injury. Therefore, an effective carrier with efficient load rate, sustained drug release profile, and prominent repair effect is urgent to be developed. In this study, we have prepared a bionic multichannel Tubasatin A loaded nanofiber conduit (SC-TUBA(+)) through random electrospinning and post-triple network bond crosslinking for inhibiting HDAC6 as well as promoting axonal regeneration during spinal cord injury treatment. The Tubasatin A-loaded nanofibers were shown to be successfully contained in poly(glycolide-co-ε-caprolactone) (PGCL)/silk fibroin (SF) matrix, and the formed PGCL/SF-TUBA nanofibers exhibited an uniform and smooth morphology and appropriate surface wettability. Importantly, the TUBA loaded nanofibers showed a sustained-release profile, and still maintains activity and promoted the extension of axonal. In addition, the total transection large span model of rat back and immunofluorescent labeling, histological, and neurobehavioral analysis were performed for inducing spinal cord injury at T9-10, evaluating therapeutic efficiency of SC-TUBA(+), and elucidating the mechanism of TUBA release system *in vivo*. All the results demonstrated the significantly reduced glial scar formation, increased nerve fiber number, inhibited inflammation, reduced demyelination and protected bladder tissue of TUBA-loaded nanofibers for spinal cord injury compared to SC-TUBA, SC and Control groups, indicating their great potential for injured spinal cord healing clinically.

1. Introduction

Spinal cord injury (SCI) results in partial or complete loss of motor and sensory function of the limbs below the plane of neurological injury, which imposes a huge economic burden on the patient and society [1]. The ineffective regeneration for axons is a major obstacle to the functional recovery of central nervous system (CNS) in mammals [2–4]. Insufficient intrinsic growth capacity of damaged neurons, glial scarring,

fragmentation of myelin sheath, and even inhibitory factors associated with axonal components may lead to ineffective axon regeneration [5–7]. Although some previous reports have shown that partial axonal regeneration can be improved by removing or neutralizing these above inhibitors. However, the effect of regeneratiom is unobvious [8–10]. Therefore, an effective drug-loaded scaffold is urgently for the reparing of large spinal cord defect.

Tubasatin A (TUBA), which is a potent selective histone deacetylase 6 (HDAC6) inhibitor with tetrahydro-γ-carboline capping, can promotes axonal regeneration and improves behavioral function in mammals [11, 12]. It has been reported that inhibition of histone deacetylases (HDACs) promotes histone acetylation as well as present neuroprotective effects in various disease models associated with neurodegeneration [13–16]. Among them, HDAC6 is a microtubule-associated deacetylase, which is a potential target for protection and regeneration after neurological injury [12,17,18]. Despite the important role of TUBA in promoting axonal regeneration and stabilizing microtubules in spinal cord injury repair, the high outflow rate, limited brain penetration (B/P = 0.15), and low uptake rate (<100 ng/g) have limit the clinical application of TUBA [19, 20]. In addition, TUBA also exhibits permeability to the blood-brain barrier, but the results of the previous report suggest that its percentage of passing through is still very limited [19]. So, sustained, higher peripherally administered concentrations are required to exert neuroprotective effects. This multiple and complicated injection operation increases the risk of infection, and it is not easy to control the concentration of TUBA. More importantly, local blood circulation is impaired after spinal cord injury, making it difficult for TUBA to really enter the deeper part of the spinal cord injury area and achieve the ideal therapeutic effect. These factors severely limit the application of TUBA in the treatment of spinal cord injury. Therefore, it is important to design a feasible local drug delivery system for the clinical application of TUBA in the treatment of spinal cord injury.

Electrospinning is a simple and widely used technique for the continuous extraction of nanofibers from viscoelastic fluids by electrostatic repulsion between surface charges, which can be assembled into ordered or graded structures depending on different arrangements, stacking and folding [21]. In recent years, electrospun fiber as drug delivery systems have received increasing attention due to the unique properties of electrospun fibers such as great specific surface area and very high porosity [22]. To obtain better drug-polymer compatibility and improve drug activity, polymer-blended drug delivery systems have been promoted [23–26]. Although electrospun nanofibers show great potential for applications in biomedical research, the structure and composition of polymeric nanofibers for tissue regeneration scaffolds need to be further optimized. Further still, it has been reported that electrospun nanofiber scaffolds provide physical cues that can guide the extension of neurites from dorsal root ganglia (DRG) and embryoid bodies (EBs) and also further increase the length of neurites through functionalization [27–30]. Therefore, a wide variety of natural and synthetic polymers have been electrostatically spun into fibers for local drug delivery. Among them, poly(glycolide-co-ε-caprolactone) (PGCL) has attracted much attention due to its elasticity similar to rubber, amorphous nature and rapid biodegradability, as well as its ability to enhance intercellular interactions [31–33]. In addition, silk protein (SF) exhibits prominent biocompatibility, controlled biodegradability, absorbability of natural proteins, low immunogenicity for applications in both tissue engineering and drug release [34–37]. Based on these advantages, we will prepare a hybrid PGCL/SF-TUBA multi-channel bioactive filament nanofiber catheters via combine electrospinning technique and post-network bond processing, which may be a useful strategy for more loaded active factor in neural tissue engineering applications.

2. Materials and methods

2.1. Materials

Poly(glycolic acid-co-ε-caprolactone) (PGCL, weight-average molecular weight = 100,000 g/mol) with a glycolic acid/ε-caprolactone ratio of 50:50 and Tubasatin A (TUBA, purity>99.9%) were purchased from Shenzhen Mai Qi Biomaterials Co., Ltd. (Shenzhen, China) and Sigma-Aldrich Trading Co., Ltd. (Shanghai, China), respectively. Silk fibroin (SF) is an extract from silkworm cocoons in our laboratory. PC12 cells for *in vitro* experiments were obtained from Shanghai Cell Bank of Chinese Academy of Sciences (Shanghai, China). Cell counting kit (CCK-8) was obtained from Sigma-Aldrich Trading Co., Ltd. (Shanghai, China). Dulbecco's modified eagle medium (DMEM), Fetal bovine serum (FBS), and antibiotic-antibacterial medicine (penicillin/streptomycin) were purchased from Hyclone Trading Co., Ltd. (Shanghai, China). Hexafluoroisopropanol (HFIP, purity≥99.56%) was obtained from Shanghai Darui Fine Chemicals Co., Ltd. (Shanghai, China). Unless otherwise specified, all the above reagents were used directly. All the materials were used as received, except where mentioned otherwise.

2.2. Preparation of multichannel nanofiber conduit

PGCL and extracted SF were mixed and then dissolved in 10 mL HFIP at a mass ratio of 5:5, formed a mixture with 10% concentration. After stirring until clarified, quantitive TUBA was added in the above-clarified mixture forming electrospinning solution with a relative mass fraction ($W_{TUBA}/(W_{PGCL + SF})$) of 1%. After mixing, the solution was continuously stirred by a stirrer for 2 days till completely dissolved. Followed by ultrasonic treatment to completely dissolve and remove any air bubbles. The electrospun solution was prepared into random fiber by a conventional electrospinning device, which was composed of a propulsion pump, a high pressure supply and a metal collector. The spinning parameters were set to an output voltage = 10.3 kV, the distance from the needle tip to the receiver was 18 cm, and the propulsion speed of the propulsion pump was set to 0.8 mL/h. The parameters were no longer adjusted during electrospinning to ensure that stable fiber scaffolds were obtained. The obtained electrospun nanofiber scaffolds were crosslinked by glutaraldehyde vapor (evaporation in 25% glutaraldehyde aqueous solution) at room temperature for 4 h. Finally, the nanofiber scaffolds were vacuum dried at room temperature for 7 days to prepare for the next step of characterization and testing. Singlechannel PGCL/SF nanofiber conduit (SC), singlchannel PGCL/SF-TUBA nanofiber conduit (SC-TUBA), and multichannel PGCL/SF-TUBA nanofiber conduit (SC-TUBA(+)) were prepared for animal experiments.

2.3. Characterization and testing

The morphology of the nanofibers after gold spraying was observed by scanning electron microscopy (SEM, Phenom XL, Netherlands) operating with sputter gold plating for 35 s at 5 mA at an accelerating voltage of 10 kV. A contact angle measuring device (JC 2000D 2 A, Shanghai Zhongchen Digital Technology Equipment Co., Ltd, China) was used to testing the wettability of prepared nanofibers scaffolds. In this testing, 0.02 mL deionized water was added to the sample and three different positions of the sample were taken to test the water contact angle and calculate the average value. Image-J (USA) was adopted to determine the diameter of nanofibers, inner diameter and wall thickness of nanofibers scaffolds.

2.4. TUBA sustained release testing in vitro

SC-TUBA (weight: 2.055 ± 0.065 μg, n = 3) with 1 mL of phosphate buffered salt (PBS, Gibco, C10010500BT) was taken to determine the

effect of TUBA release *in vitro* from the nanofibers. The SC-TUBA with PBS were placed in a rotary shaker at 50 rpm and 37 °C 500 μL of supernatant containing released TUBA was removed and stored at −20 °C at the set time points on days 1, 3, 6, 9, 12, 15, 18, 21, 24, 27, and 30, following supplemented with equal amounts of PBS. The concentration of TUBA in the supernatant was measured using HPLC and expressed as the cumulative amount of TUBA released over time according to the formula in previous reported literature [38,39].

2.5. Cytocompatibility in vitro

2.5.1. Cell culture

PC12 cells were cultured and proliferated in a suitable environment of 37 °C, 5% CO_2, 95% air. The culture medium was RMPI 1640 medium (GIBCO, C11875500BT) containing 10% fetal bovine serum (GIBCO, 10099–141) and 1% penicillin/streptomycin (GIBCO, 15140–122). PC12 cells was induced to differentiate into neuron-like cells with β-NGF (50 ng/mL, Sino Biological, 11050-HNAC-3).

2.5.2. Cell value-added-toxicity assay

Cell suspensions were obtained by digesting β-NGF-induced differentiation of PC12 cells with 0.25% EDTA trypsin (GIBCO, 25200056), adding cell suspensions to 96-well plates at 1×10^4 cells per well and supplementing the outermost wells with 100 μL of PBS to prevent the outermost medium from evaporating during the incubation process. To test cell activity after experimental treatment, drug-containing medium was discarded and 100 μL of fresh medium was added to each well, followed by the addition of 10 μL of Cell Counting Kit 8 (CCK-8) solution (Meilunbio, CCK8-500 T) to each well, followed by incubation in an incubator for 3 h. Finally, the absorbance of each well at 450 nm was measured using an enzyme marker. Five replicate wells were set up for each group of cells.

Add 2×10^4 β-NGF-induced differentiated PC12 cells to 24-well plates, SC and SC-TUBA extracts were pretreated for 12 h. Cells were co-incubated for 2 h using an equal volume of EdU ($1 \times$, 10 μm) in BeyoClickTMEdU-555 Cell Proliferation Assay Kit (Beyotime, C0075L), paraformaldehyde solution (4% PFA, biosharp, BL539A) for 1 h at room temperature, wash and add PBS containing 0.3% Triton X-100 for 15 min at room temperature, wash and add Click reaction solution for 30 min at room temperature and avoid light, shake gently to ensure that the reaction mixture can evenly cover the cells, aspirate the wash solution and add Hoechst 33,342 ($1 \times$) was added to each well and incubated for 10 min at room temperature and protected from light.

2.5.3. Bioactivity evaluation of Tubastatin A

The supernatants of SC and SC-TUBA were collected on day 3 and used to assess the biological activity of TUBA released from the nerve conduits. PC12 cells was added to 12-well plates pre-coated with poly-Lysine (Solarbio, P2100-10) and incubated at 37 °C and 5% CO_2, supplemented with 1 mL of RMPI 1640 medium containing 10% fetal bovine serum, 1% penicillin/streptomycin and 50 ng β-NGF to each well. Medium was changed every 2 days and the experimental group drug was added on day 3. An equal volume of PBS was added to the blank group and incubated in the incubator for 12 h.

2.5.4. Cell adhesion assay

Round slides (Φ10 mm) were prepared as described above, sterilized and grouped into 24-well plates, and 2×10^4 PC12 cells were inoculated onto each slide, supplemented with 1 mL of RMPI 1640 medium containing 10% fetal bovine serum, 1% penicillin/streptomycin and 50 ng β-NGF. After 3 days of incubation, the slides were washed with PBS at room temperature and a sufficient amount of electron microscopy fixative (Servicebio, G1102) overnight. After aspiration and dehydration with gradient ethanol solutions (30%, 50%, 70%, 90%, 95%, and 100%),

the slides were finally dried in a lyophilizer (Labogen, CS55-4, Denmark) for 4–6 h. After gold spray treatment, the cell adhesion on the slide surface was observed under SEM.

2.5.5. Immunocytochemistry

After 72 h of *in vitro* incubation, the cultures were fixed in paraformaldehyde solution (4% PFA, biosharp, BL539A) for 15 min, washed with PBS, permeabilized with PBS containing 0.3% Triton X-100 for 20 min at room temperature, closed with goat serum (GIBCO, 16210064) for 30 min at room temperature, and stained with Anti-beta III Tubulin antibody (EP1569Y, 1:500, Abcam, United States) was immunostained overnight at 4 °C, the antibody was removed and washed with PBS, then incubated with Goat Anti-Rabbit lgG H&L (Alexa Fluor ®488,1:200,Abcam, United States) at room temperature for 1.5 h. All neurites in the wells were observed using a fluorescence microscope (IX73 + DP80). Neurosynaptic extension of β-NGF-induced differentiation of PC12 cells was quantified using Image-J software.

2.6. Animal experiments

All rats were obtained from Shanghai Slaccas Experimental Animal Co., Ltd (Shanghai, China) and all experimental schemes are in agreement with the requirements of the Institutional Animal Care and Use Committee (IACUC) of Shanghai Jiao Tong University School of Medicine Affiliated Shanghai Sixth People's Hospital (Fengxian Hospital) by IACUC. Ethical principles were followed throughout the experiment. All experimental plans were proceeding to conform to the Animal Management Regulations of China (1988 and revised in 2001, Ministry of Science and Technology).

In this experiment, 200 ± 20 g adult female SD rats were subjected to spinal cord transection transplantation and randomly divided into four groups: spinal cord injury group (Control, n = 10), single-channel catheter scaffold group (SC, n = 10), single-channel bioactive silk nanofiber catheter scaffold equipped with TUBA (SC-TUBA, n = 10), and multiple-channel bioactive silk nanofiber catheter scaffold equipped with TUBA (SC-TUBA(+), n = 10). All rats were anesthetized by intraperitoneal injection of 10% chloral hydrate solution (400 mg/kg, Sigma-Aldrich, 23,100), the lamina was excised to expose the dorsal aspect of the T9-10 segment, and the spinal cord was transected with microscissors to form a 5 ± 0.5 mm gap, and the wound was hemostatic. Then the material was implanted into the transected gap with microscopic forceps and ensured that it coincided with the lesion cavity, and the muscle and skin were sutured layer by layer after checking for correctness. To prevent infection, all animals were given amoxicillin (10 mg/kg, Chinese national drug) intraperitoneally for 1 week after surgery. Food and water were easily accessible to all animals, and manual bladder massage was performed twice daily until the urinary reflex was restored.

2.6.1. Neurobehavioral testing

Neurobehavioral recovery after spinal cord injury in rats was assessed using Basso, Beattie and Bresnahan (BBB) scores. Scores were observed at specific time points by two independent observers who had no knowledge of the experiment. Animals were placed in the center of an open floor and scores were recorded strictly based on observation. Each animal was observed and scores were recorded for no less than 4 min per week. postoperatively once a week until 8 weeks postoperatively.

2.6.2. Histology and immunofluorescence staining

The animals were anesthetized and executed with an overdose of 10% chloral hydrate at 8 weeks postoperatively, the hearts were opened and fully exposed, and all rats were perfused with pre-warmed 0.9% saline (pH = 7.3) for 5 min, then perfused with pre-cooled 4% paraformaldehyde (4% PFA, biosharp, BL539A) for 6 min. The samples were fixed in 4% paraformaldehyde for 24 h at 4 °C, then dehydrated in a

gradient of 20%–30% sucrose solution in turn, and frozen sections were embedded in OTC (Servicebio, G6059-110 ML) with a section thickness of 10 μm, numbered and labeled, and stored at −20 °C.

Immunofluorescence staining was performed using standard protocols, and sections were incubated with anti-glial fibrillary acidic protein (GFAP; 1:400; Abcam), anti-neurofilament 200 (NF200; 1:1000; Abcam), and macrophage anti-CD68 (1:100; Santa Cruz) overnight at 4 °C. After 3 shaking washes with PBS (pH = 7.4) on a decolorization shaker and incubation with Alexa Fluor546 (1:300; Abcam) or Alexa Fluor488 (1:300; Abcam) secondary antibody for 50 min at room temperature protected from light, all specimens were washed 3 times with PBS and 4′,6-diamidino-2-phenylindole (DAPI; Servicebio; G1012) to restain the nuclei, and the sections were slightly shaken and then sealed with anti-fluorescence quenching sealer (Servicebio; G1401). Sections were observed and images were acquired under an orthomosaic microscope model (NIKON Eclipse ci), and each index was photographed using the same parameter settings, and then quantitative analysis was performed using Image-J software.

2.6.3. LFB staining

Spinal cord samples were obtained according to the method described previously, and continuous cross-sectional sections of 5 μm thickness were prepared from both sides of the injury junction, and the sections were dewaxed to water by xylene (Sinopharm Chemical Reagent Co., Ltd.; 10023418) and anhydrous ethanol (Sinopharm Chemical Reagent Co., Ltd.; 100092683) sequentially, and stained with myelin staining solution set (Servicebio. G1030) at 60 °C, repeatedly differentiated water washing and microscopic examination until the myelin sheath was blue background nearly colorless. Sections were oven dried at 65 °C, cooled and then re-stained with 95% ethanol in eosin, and then sealed sequentially by anhydrous ethanol (Sinopharm Chemical Reagent Co., Ltd., 100092683) and xylene (Sinopharm Chemical Reagent Co., Ltd., 10023418) dehydrated neutral gum. Three sections of the spinal cord of each animal (including the section in the epicenter) were evaluated for LFB-positive areas, microscopically examined with an orthomosaic microscope model (NIKON Eclipse ci), and the remaining myelin area in the anterior and posterior horn of the spinal cord was quantified by determining the integrated optical density (IOD) of the remaining myelin in selected areas using Image-J software.

2.7. Statistical analysis

All analyses were performed using the SPSS 25.0. Data were expressed as mean ± SD. Statistical comparisons between the two groups
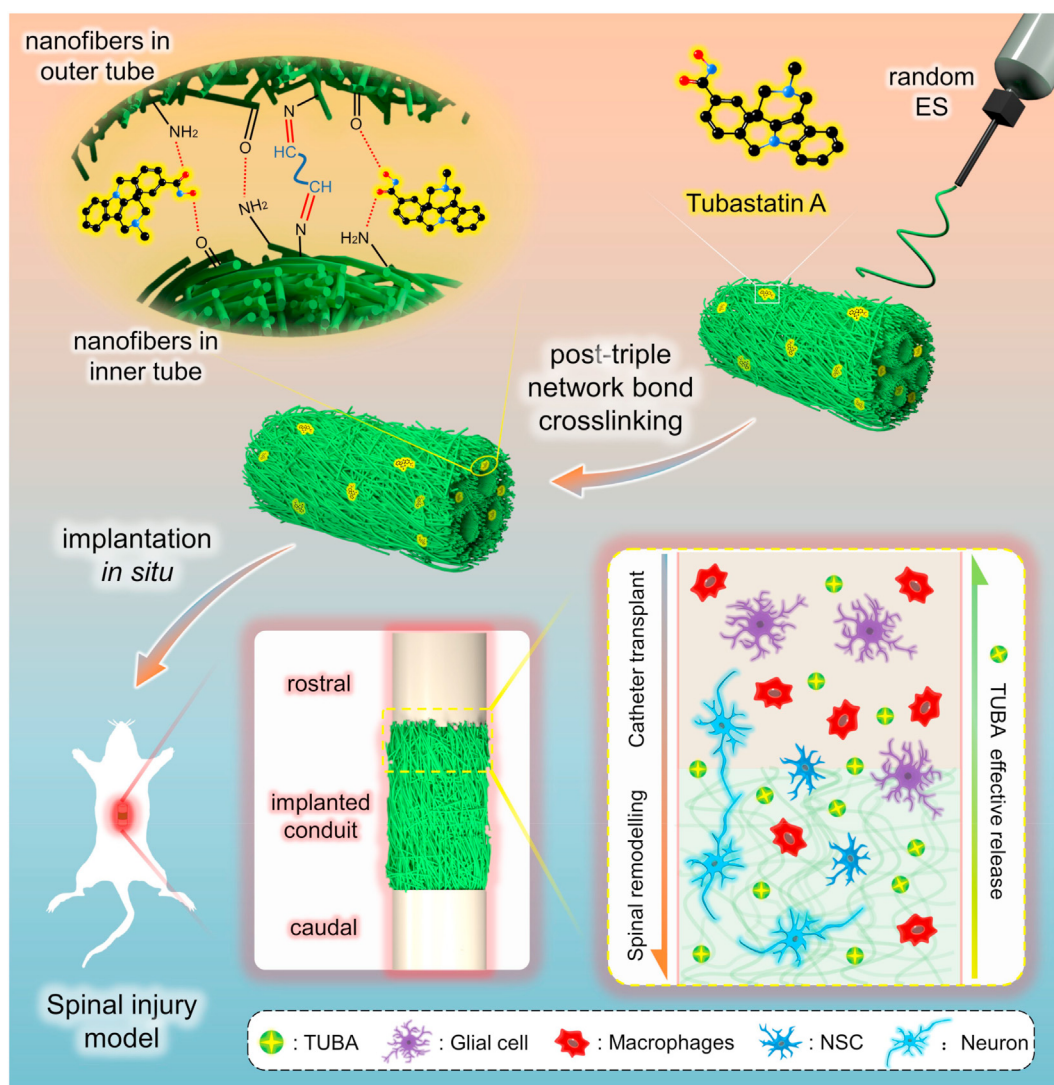

Fig. 1. Schematic illustration of the preparation for the bionic multichannel nanofiber conduit carrying Tubastatin A (SC-TUBA(+)) by random electrospinning and post-triple network bond crosslinking (amidation, Schiff based reaction, and hydrogen-bonding network densification) and its effective implantation in spinal injury model in rat.

were performed using the two independent-samples *t*-test and the inter group were performed using the One-way analysis of variance (ANOVA). (two-tailed) p < 0.05 was considered to be statistically significant.

3. Result

As in Fig. 1, a bionic multichannel TUBA loaded nanofiber conduit (SC-TUBA(+)) have been prepared via random electrospinning and post-triple network bond crosslinking (amidation, Schiff based reaction, and hydrogen-bonding network densification) for inhibiting HDAC6 as well as promoting axonal regeneration during spinal cord injury treatment. Subsequently, the prepared TUBA-loaded nanofiber conduit may effectively promote neuronic induction, spinal regeneration after SCI, and some improvement of bladder loss compensation when implanted with SC-TUBA(+) in the treatment of large spinal cord injury. In brief, we have designed and proposed a new mode for the loading and delivery of TUBA, which can help promote the clinical development and application of TUBA in the field of neural repair.
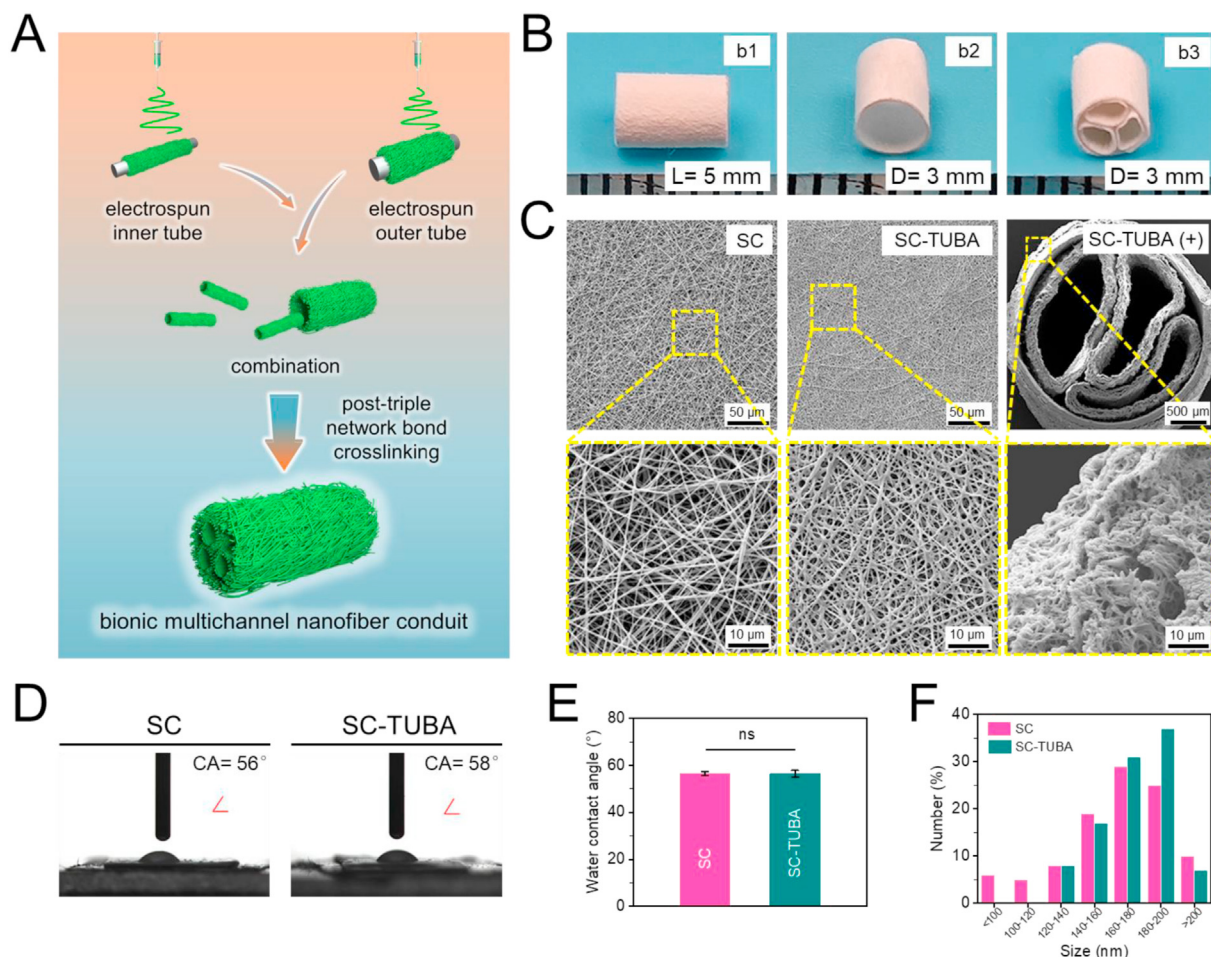

Fig. 2. (A) Schematic diagram of the fabrication of the bionic multichannel nanofiber conduit based on PGCL/SF nanofibers. (B) The appearance images of SC-TUBA and SC-TUBA(+). (C) SEM images of SC, SC-TUBA, and SC-TUBA(+). (D) and (E) Water contact angle images of PGCL/SF nanofiber and PGCL/SF-TUBA nanofibers. (F) Diameter distribution of PGCL/SF nanofiber and PGCL/SF-TUBA nanofibers. (ns: not significant).
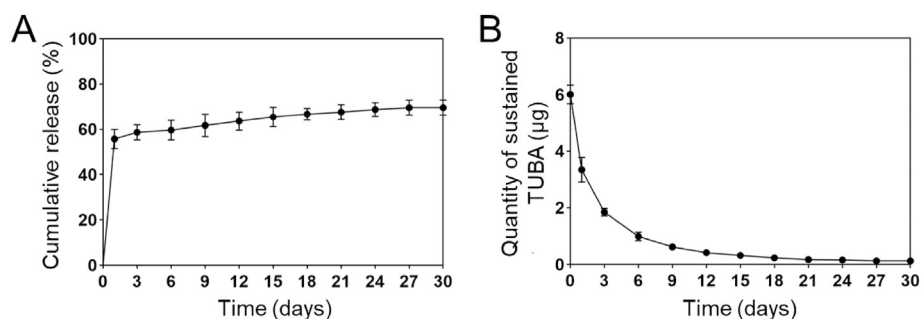

Fig. 3. In vitro releases of TUBA from SC-TUBA nanofibers in pH = 6.8 PBS (n = 5). (A) Cumulative release rate, and (B) the quantity of sustained TUBA in set time points.

3.1. Microstructure and surface wettability of nanofibers

The bionic multichannel nanofiber conduit was prepared as described above (Fig. 2A). The microstructure and morphology of the nanofiber conduits were examined using scanning electron microscopy (SEM), and high-density interwoven nanofiber structures were observed in both SC and SC-TUBA groups (Fig. 2C). Among them, the nanofiber diameter interval of SC and SC-TUBA was about 140–200 nm. The diameters of prepared fiber between the two groups was not statistically significant,

indicating that loaded TUBA in PGCL/SF matrix did not change the arrangement of the nanofiber structure. The wettability of the scaffold materials was assessed by contact angles (as in Fig. 2D and E), which were 56.58° for SC and 56.42° for SC-TUBA, respectively. Both θ < 90°, indicating that both are hydrophilic materials.

3.2. TUBA release properties of nanofibers

The release of TUBA from SC-TUBA nanofibers under physiological
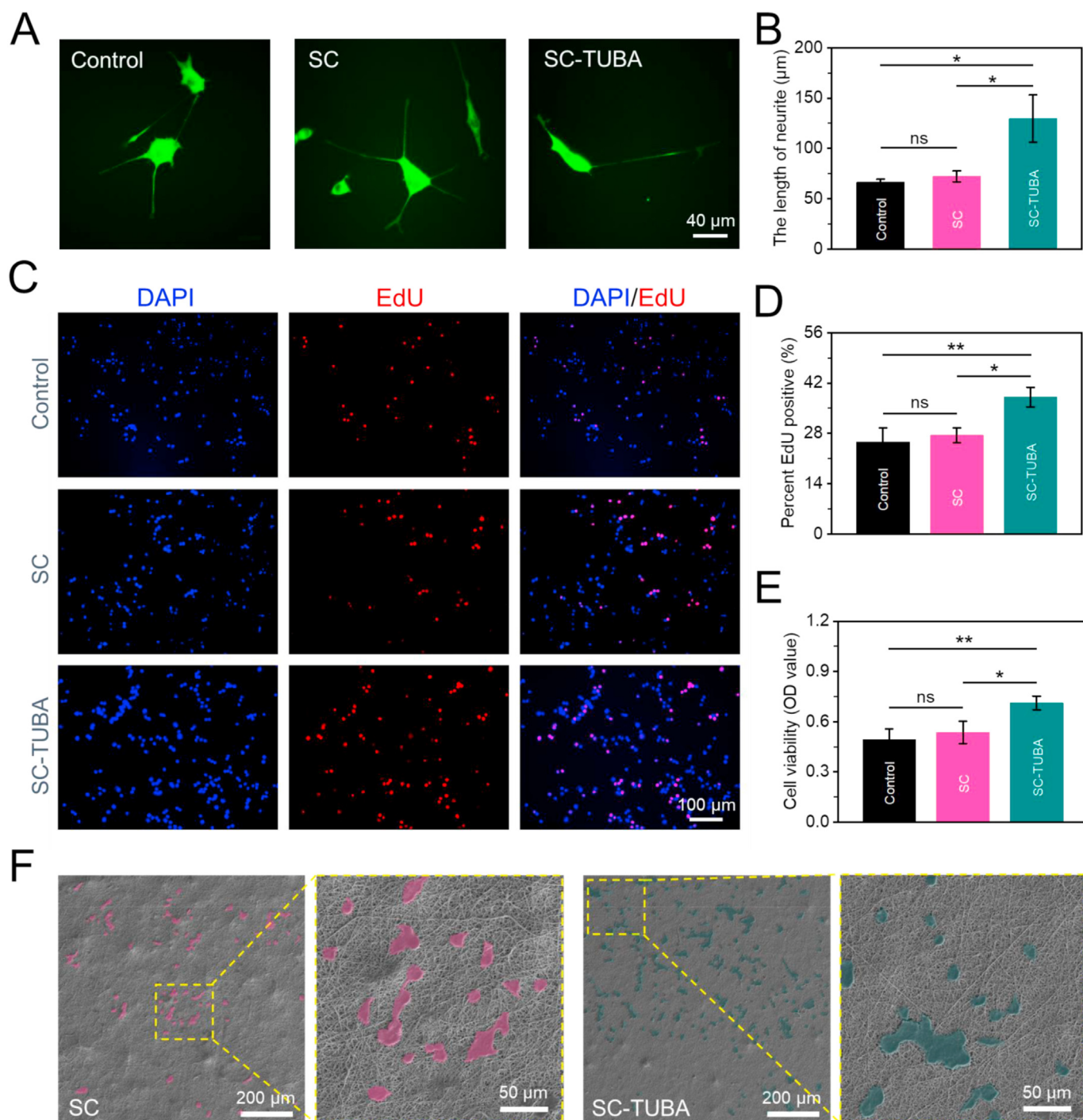

Fig. 4. Effects of SC-TUBA on cell activity and adhesion. (A) Staining on nerve filament of differentiated PC12 cells on the surfaces of SC-TUBA nanofibers. (B) The length of nerve filament in each group using Image-J software quantitative analysis. (C) and (D) Effects of EdU on the activity of differentiated PC12 cells with SC and SC-TUBA. (E) Effects of CCK-8 on the activity of differentiated PC12 cells with SC and SC-TUBA. (F) SEM images of SC and SC-TUBA cell adhesion. NS, not significant; $*P < 0.05$; $**P < 0.01$.

conditions was analyzed using HPLC. As shown in Fig. 3, during the 30-day release experiment, the drug showed a violent release on the first day, followed by a continuous slow release. Thus, approximately 70% of TUBA was released from the stent in the SC-TUBA bionic nerve conduit.

3.3. The activity and facilitates neurosynaptic extension of nanofibers in vitro

In vitro, differentiated PC12 cells were cultured by dip in SC and SC-TUBA to determine whether the released TUBA retained biological activity. Immunofluorescence results showed insignificant neurite growth in PC12 differentiated cells in the SC group compared to the Control group and neurite growth in the SC-TUBA group (Fig. 4A and B). CCK-8 (Fig. 4E) and EdU (Fig. 4C) results indicated that SC was not significantly cytotoxic and that SC-TUBA increased the activity of PC12 differentiated cells (Fig. 4D). Cell adhesion experiments showed that both SC and SC-TUBA could provide attachment for cells, and the addition of TUBA in SC nanofibers did not have a significant effect on cell adhesion (Fig. 4F). This suggests that TUBA released from the SC-TUBA remained active and promoted neurosynaptic proliferation.

3.4. Evaluation of spinal cord repair in vivo

The results of positive NF200 neurofilaments (NF200, a marker for neuronal and axonal regeneration) at different locations of spinal cord injury were quantified to assess the effect of SC-TUBA(+) on nerve axon regeneration *in vivo*. The effect of nerve tissue regeneration after nerve conduit implantation was assessed at week 8, and NF200 cell density was significantly increased in the SC-TUBA(+) group compared with the SCI group ($P < 0.01$). The mean neurofilament density in the SC-TUBA(+) group was $33.303 \pm 2.996\%$ in the Rostral region (Fig. 5B) and Caudal region (Fig. 5C) $21.4935 \pm 4.0195\%$. The addition of TUBA seemed to promote the increase of neurofilaments, and based on these data, local delivery of TUBA from the SC-TUBA(+) bionic nerve conduit scaffold after SCI increased neurosynaptic regeneration at the injury site.

The extent of astrocyte aggregation was quantified by detecting the density of GFAP staining (Fig. 6A). After 8 weeks of injury, the Control group saw GFAP$^+$ cell aggregates around the lesion, leaving poorly repaired cavities with only a small amount of NF200 (Fig. 6A). These astrocytes were tightly packed to form a scar barrier and hindered neural tissue regeneration. Compared with the Control group, the SC-TUBA(+) and SC-TUBA groups showed less pronounced proliferation of reactive astrocytes and decreased GFAP expression around the injury site after
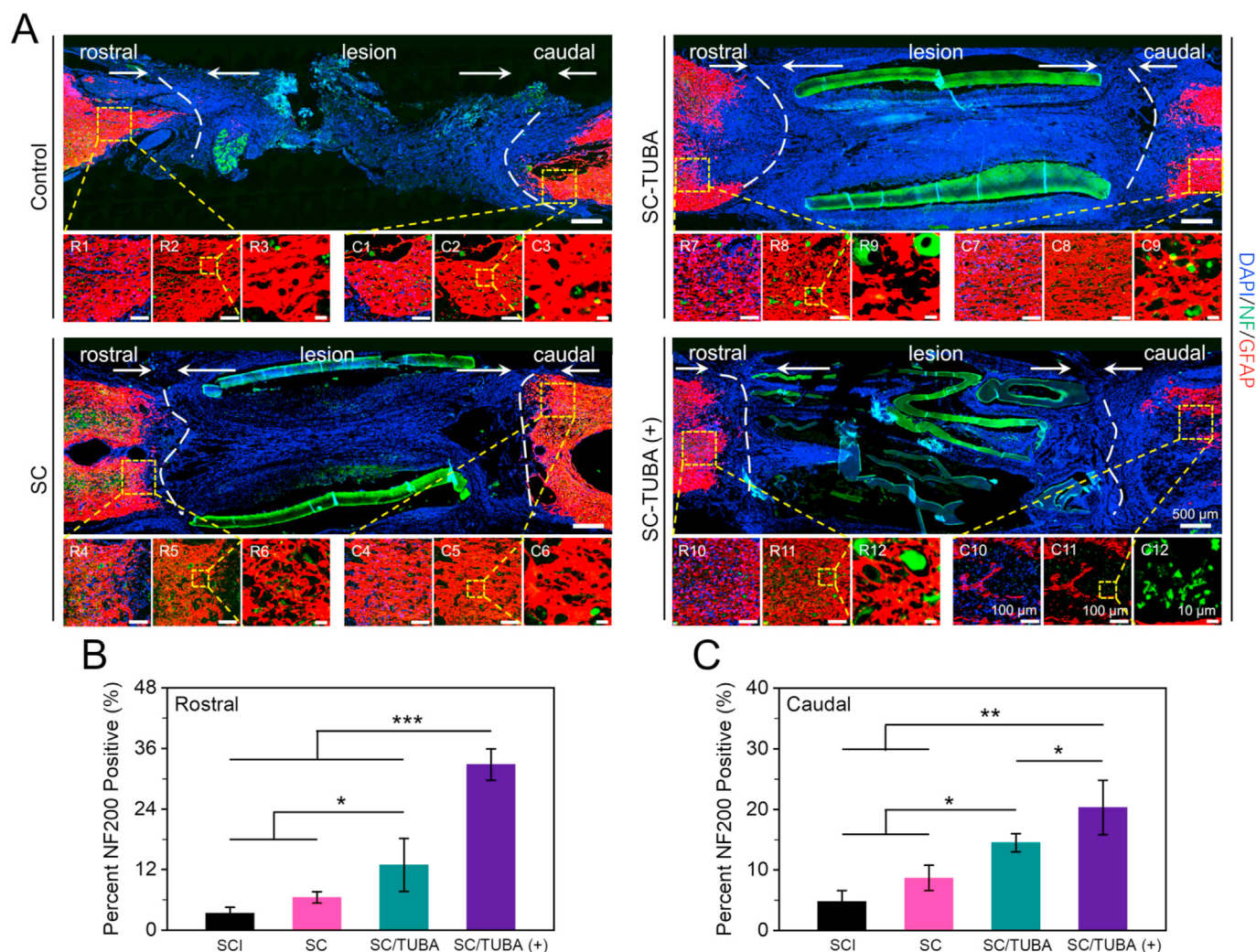

Fig. 5. Spinal cord tissue was regenerated 8 weeks after modeling. (A) Control group, SC group, SC-TUBA group and SC-TUBA(+) group representative images showing nerve filament (NF200, green) and glial fibrillary acidic protein (GFAP, red) staining. The white dotted lines in the full view represent the cross-cut lesion area, the arrows represent the rostral lesion and the tail, and the yellow dotted boxes show enlarged Rostral (R1-3,R4-6,R7-9,R10-12) and Caudal (C1-3,C4-6,C7-9,C10-12) areas. Image-J software for quantitative analysis of rostral (B) and tail (C) caudal. ns, $*P < 0.05, **P < 0.01, ***P < 0.001$.

treatment. GFAP expression was significantly reduced after local application of SC-TUBA(+), which induced a more significant reduction than that in the SC-TUBA group, effectively preventing the excessive aggregation of astrocytes. Thus, local delivery of MC-TUBA attenuated the proliferation of glial cells at the injury site.

Infiltration of inflammatory cells around the lesion is an important signal in response to chronic inflammation. Staining of activated macrophages by anti-CD68 antibody (Fig. 6B) was used to assess the activity of macrophages at the lesion site after SCI. After 8 weeks of injury, the infiltration of CD68$^+$ cells was reduced to different degrees in the SC-TUBA and SC-TUBA(+) groups compared with the Control and SC groups, and the effect was more pronounced in the SC-TUBA(+) group, confirming the inhibitory effect of this delivery system on inflammation after SCI.

Luxol Fast Blue (LFB) staining was performed to assess the myelin protective effect of SC-TUBA(+) on the anterior and posterior horn of the injured spinal cord (as in Fig. 7). A large number of cellular debris and degenerated axons were present near the epicenter of the spinal cord transection injury. As assessed by IOD, myelin showed a protective effect in the SC-TUBA(+) group compared to the Control group (Fig. 7C and E). The SC-TUBA(+) group showed a better protective effect compared to the SC-TUBA group. Based on these results, local administration of SC-TUBA(+) attenuates the demyelinating effect after SCI.

At week 8 after SCI, the injured spinal cord was excised from the experimental animals and the effect of SC-TUBA(+) on the lumen was observed by H&E staining of horizontal sections (Fig. 8A). As shown in the figure, incompletely degraded nerve conduit scaffolds were visible in the epicenter of SC, SC-TUBA and SC-TUBA(+) groups. Compared with Control group, SC, SC-TUBA and SC-TUBA(+) groups all showed different degrees of guidance function, and SC-TUBA(+) group significantly reduced the regeneration of abnormal scar tissue.

Functional assessment of the hind limbs of the rats was performed weekly by two uninformed examiners using the BBB scale. All groups of rats were completely paralyzed immediately after modeling, and the BBB scores were significantly higher in the SC-TUBA and SC-TUBA(+) groups than in the Control group (Fig. 8E). In addition, the BBB score was higher in the SC-TUBA(+) group (9 ± 1 point) than in the SC-TUBA group (7.5 ± 0.5 points). Therefore, TUBA had a positive effect on rats after SCI, while SC-TUBA(+) treatment promoted the recovery of hindlimb function in rats after SCI.

Urinary tract disorders are a serious complication of SCI and can cause irreversible pathological changes in the bladder, affecting the quality of life and overall survival of patients with SCI. Effective relief of urinary tract damage depends on the recovery of spinal cord neurological function, and is therefore another important indicator of treatment efficacy. bladder volume in the Control group increased significantly within 8 weeks after SCI, while the bladder of rats in the SC-TUBA(+) group was closer to normal (Fig. 8B). H&E staining showed that SC-TUBA(+) was effective in preventing pathological damage such as severe bladder wall thickening and muscle bundle disorder (Fig. 8C) The implantation of SC-TUBA(+) provided effective protection to the urinary system and further demonstrated the effect of neural repair.

4. Discussion

Spinal cord injury is one of the most serious public health problems, yet effective treatment measures remain to be explored [40,41]. Following spinal cord injury, scar formation at the injury site and the limited ability of neuronal axons to regenerate make recovery from spinal cord injury difficult [8,42]. Studies have shown that HDAC6 expression levels are significantly upregulated in damaged neurons and that inhibition of HDAC6 promotes neuronal survival and regeneration [18,43, 44]. TUBA, a potent and selective HDAC6 inhibitor, is much more selective than all other isozymes and is of great research value in spinal cord injury repair [11,20]. By inhibiting HDAC6 expression levels, the aim of promoting spinal cord injury repair can be achieved [12,14,16].
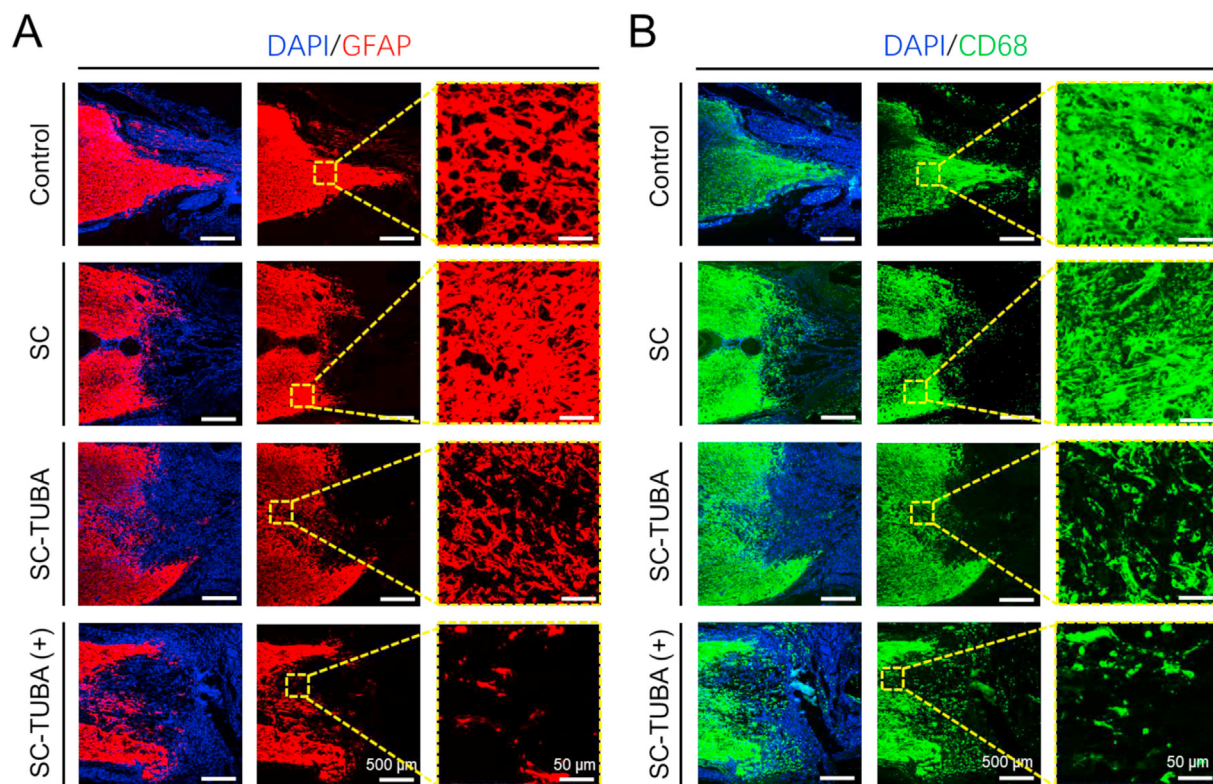

Fig. 6. Local SC-TUBA(+) administration reduced glial scar formation and inhibited inflammation in Control group, SC group and SC-TUBA group. (A) SC-TUBA(+) group after rostral treatment GFAP fluorescence staining image. (B) SC-TUBA(+) group after rostral treatment CD68 antibody fluorescence staining image. The yellow dotted boxes show enlarged Rostral areas.
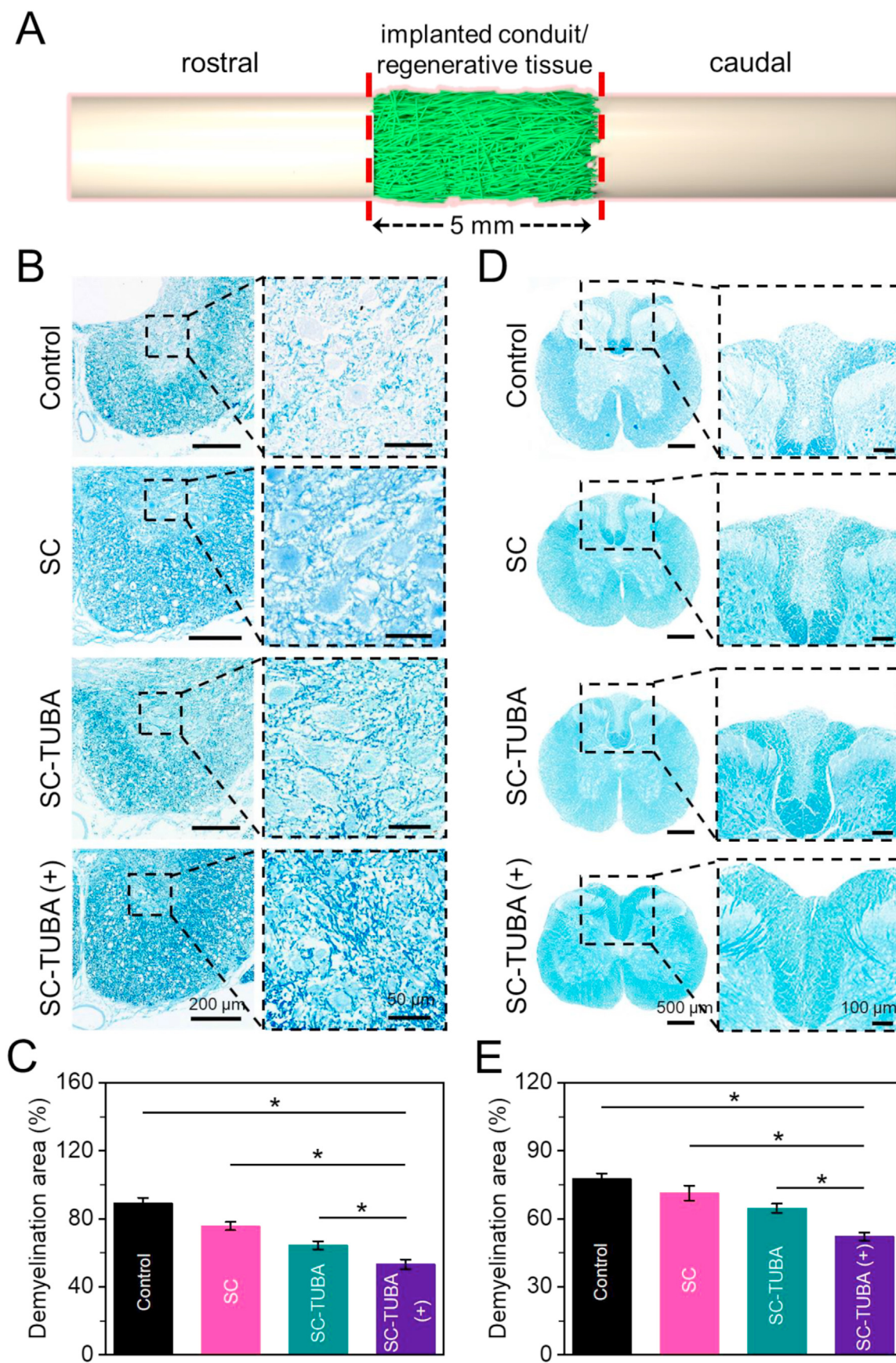
Fig. 7. MC-TUBA reduces demyelination. (A) The leading image shows the transverse view of the spinal cord (rostral injury/graft site and caudal). LFB staining for histological evaluation of the transverse view of the anterior(B) and posterior horns(D). Image-J software for demyelination of the anterior(C), posterior horns(E). (*P < 0.05).
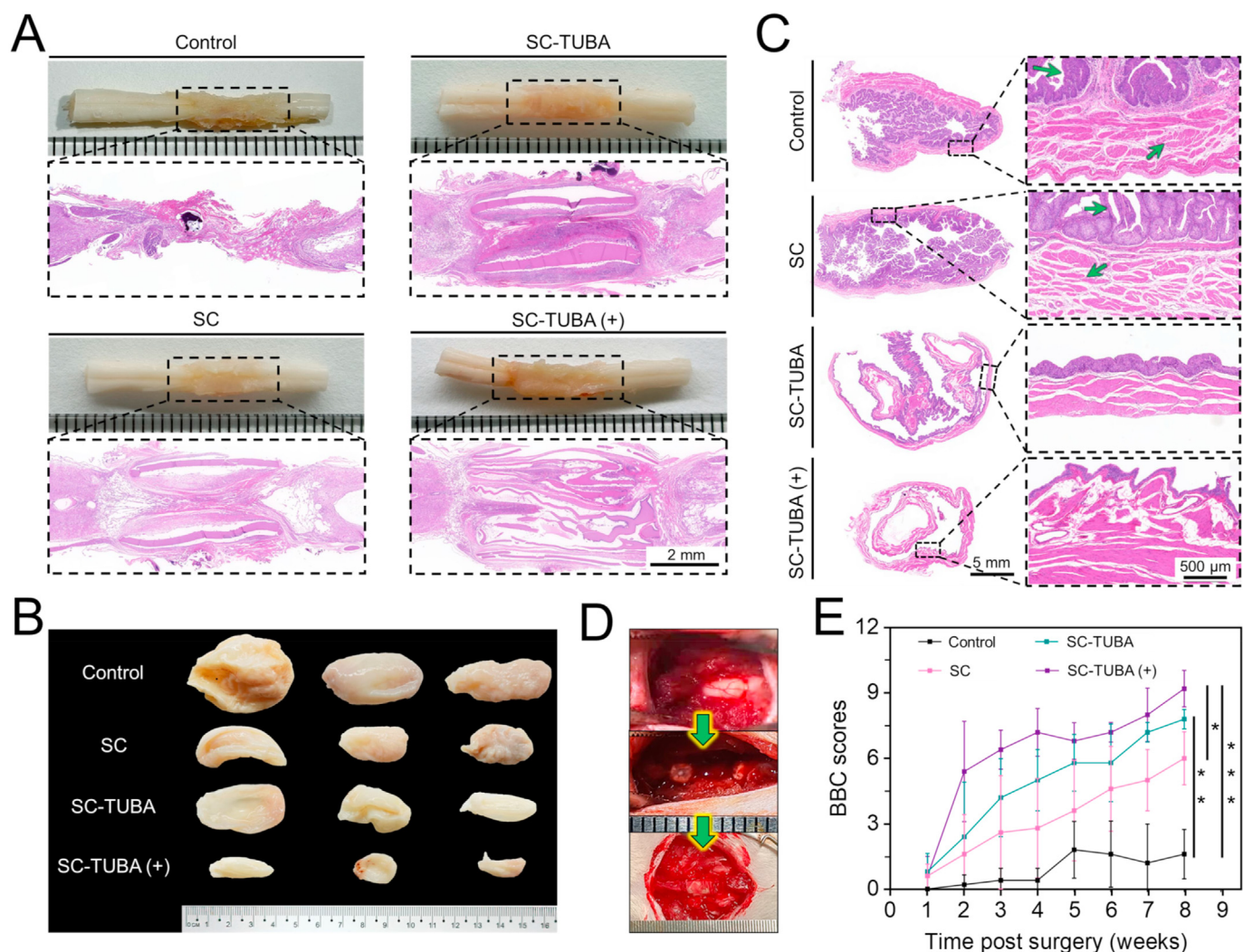
Fig. 8. Local administration of SC-TUBA(+) improves bladder decompensation and promotes functional recovery. After 8 weeks, Macromorphology of spinal cord and H&E staining (A), Macroscopic bladder morphology (B) and H&E staining (C). Green arrows indicate pathological features, transverse space of lesion is 5 ± 0.5 mm and SC-TUBA(+) implantation image (D). (E) The BBB score. (*$P < 0.05$, **$P < 0.01$, ***$P < 0.001$).

TUBA has been reported to promote axonal regeneration and functional recovery in injured mice by intraperitoneal injection [12]. However, systemic administration requires repeated applications of large doses, making it difficult to maintain relatively high concentrations locally and prone to serious side effects. Therefore, the development of long-acting release drug delivery systems (LAR-DDSs) is particularly important. Perfect DDSs maximise the therapeutic effect of the drug while minimising adverse side effects. Our results show that the constructed TUBA-loaded multi-channel bioactive nanofibrous tubular material not only avoids the disadvantages of repeated multiple intraperitoneal injections of TUBA, but also promotes axonal regeneration, reduces glial scar formation and inhibits inflammatory responses by controlling direct slow release, maximizing drug action and limiting peripheral side effects of the drug. In summary, local release of TUBA from multichannel bioactive nanofibre scaffolds has potential for preclinical studies.

Inhibitors of broad-spectrum HDACs have potential adverse effects and their safety cannot be guaranteed in many non-oncology areas, so selective HDACs inhibitors are receiving more attention. Small molecule selective HDAC6 inhibitors can promote neuronal survival and regeneration after injury. In dorsal root ganglion neurons, HDAC6 inhibitors prevent neuronal degeneration and stimulate axonal growth with fewer adverse effects, making them more suitable for clinical use [45]. Recent studies have shown that protein acetylation regulation plays an

important role in neuroprotection and in promoting the directional differentiation of endogenous neural stem cells. The selective inhibitor of histone deacetylase IIb, HDAC6, has a protective effect on nerve cell growth and promotes axonal regeneration, suggesting that HDAC6 plays an important role in the pathology of nerve injury and is a potential drug target. However, there are few effective HDAC6 selective inhibitors and their mechanism of action is unclear. TUBA, an HDAC6 inhibitor with much higher selectivity than other isozymes, is also receiving increasing attention from researchers for its role in the treatment of Alzheimer's disease, glioma and neuroprotection. Although TUBA exhibits permeability to the blood-brain barrier, studies have shown that it has a limited percentage of passage, requires sustained and high peripheral dosing concentrations to exert significant neuroprotective effects, is complicated by multiple injections, increases the risk of infection, and has unstable local concentrations during the injection interval [46–49]. More importantly, there is local blood circulation disorder after spinal cord injury, making it difficult for TUBA to really enter the deeper part of the spinal cord injury area to achieve the desired therapeutic effect. These factors have severely limited the translational clinical application of TUBA in the treatment of spinal cord injury. This study addresses these issues by loading TUBA into a multichannel bioactive nanofibrous tubular scaffold for in situ controlled release application of TUBA.

In studies on SCI, the method of TUBA administration is restricted to

intraperitoneal injection. In our study, we designed a multi-channel bioactive nanofibre tubular scaffold for TUBA delivery, namely SC-TUBA(+). This innovative vector not only overcomes the local blood circulation barrier after spinal cord injury, but also maintains a high effective local concentration of TUBA through controlled release and acts directly on the injured area, effectively promoting axonal regeneration through HDAC6 inhibition. It has been shown that reactive astrocyte proliferation after spinal cord injury includes the release of inhibitory molecules that may inhibit axonal growth, and that the application of growth-promoting therapy may reduce the inhibitory effect of astrocyte proliferation [50]. The present study showed that SC-TUBA(+) application reduced the aggregation of astrocytes around the injury site. Moreover, astrocytes are the main cells that inhibit axonal growth, which acting mainly through the secretion of chondroitin sulfate proteoglycan (CSPG) and glial scar formation, a strategy to reduce astrocyte aggregation at the injury site may mitigate these effects and thus promote potential regeneration of neural synapses. Therefore, these potential effects combined with the controlled release of TUBA may be responsible for the observed increase in nerve fibre density. In addition, SC-TUBA(+) treated animals exhibited a reduced inflammatory response at the spinal cord transection anastomosis, as determined by CD68$^+$ immunostaining of macrophages at the site of injury. This finding is consistent with previous reports that TUBA administration after spinal cord injury partially restores sci-induced autophagic flux blockade and that autophagy plays an important role in inhibiting HDAC6-induced functional recovery after spinal cord injury and supports a beneficial role of HDAC6 inhibition after spinal cord injury [12].

Spinal cord injuries often cause complications such as pain, deep vein thrombosis and urinary tract disorders. Repeated urinary tract infections and stones, as well as the inability to urinate spontaneously due to the loss of innervation of the detrusor and sphincter muscles, seriously affect the patient's quality of life and even cause long-term renal insufficiency. As a result, neurogenic bladder is one of the fatal complications for patients with spinal cord injury. The preservation and recovery of bladder tissue is a great challenge and an important indicator of the effectiveness of regenerative treatment of neural tissue. In this study, SC-TUBA(+) treatment promoted spinal cord repair and nerve regeneration, which facilitated the protection and repair of bladder tissue. The implantation of SC-TUBA(+) not only promotes the repair and regeneration of spinal nerve tissue, but also avoids complications due to pathological changes in the bladder on this basis.

5. Conclusions

Overall, local release of TUBA from the multichannel bioactive filament nanofiber catheter scaffold was achieved in a controlled manner over an extended period of time, and SC-TUBA(+)-released TUBA maintained its bioactivity *in vitro* and promoted axonal growth. Furthermore, local application of SC-TUBA(+) increased axonal extension across the injury boundary, inhibited pathological glial cell activation and inflammation, reduced demyelination, protected against bladder neurogenic loss of compensations, and promoted neurobehavioral recovery. These findings are promising, as local delivery of TUBA via a biodegradable drug delivery system implanted at the lesion site plays a beneficial therapeutic role in the repair of the spinal cord after injury. In conclusion, the local release of TUBA from a multichannel bioactive filament nanofiber catheter prepared by co-blending PGCL with SF has potential for preclinical studies.

Author statement

Conceptualization, S.Y.L., Y.H.L., Y.L.K. and Y.D.Z.; Formal analysis, Y.H.L., S.Y.L., Y.L.K., J.D., and H.T.S.; data Formal analysis, S.Y.L., Y.H.L., Y.L.K., J.D., B.T.X., C.B.L., J.D. and Y.D.Z.; Methodology, S.Y.L., Y.H.L.,Y.L.K., B.T., Y.T.C., J.C., H.T.S., J.D., and Y.D.Z.; Validation, S.Y.L., Y.H.L., Y.L.K., C.B.L., and Y.D.Z.; Visualization, B.T., Y.T.C., J.C., H.T.S.,

and B.T.X.; Funding acquisition, S.Y.L., and Y.D.Z.; Project administration, J.D., and Y.D.Z.; Supervision, Y.D.Z., and J.D.; Writing – original draft, S.Y.L.; Writing – review & editing, Y.D.Z., and J.D. All authors have read and agreed to the published version of the manuscript.

Declaration of competing interest

The authors declare that they have no known competing financial interests or personal relationships that could have appeared to influence the work reported in this paper.

Data availability

Data will be made available on request.

Acknowledgement

References

[1] H. Suzuki, T. Sakai, Current concepts of stem cell therapy for chronic spinal cord injury, Int. J. Mol. Sci. 22 (2021) 7435.

[2] M. Marcus, V. Cavalli, Intrinsic mechanisms of neuronal axon regeneration, Nat. Rev. Neurosci. 19 (2018) 323–337.

[3] B. Nieuwenhuis, A.C. Barber, R.S. Evans, C.S. Pearson, J. Fuchs, A.R. MacQueen, S. van Erp, B. Haenzi, L.A. Hulshof, A. Osborne, R. Conceicao, T.Z. Khatib, S.S. Deshpande, J. Cave, C. Ffrench-Constant, P.D. Smith, K. Okkenhaug, B.J. Eickholt, K.R. Martin, J.W. Fawcett, R. Eva, PI 3-kinase delta enhances axonal PIP 3 to support axon regeneration in the adult CNS, EMBO Mol. Med. 12 (2020), e11674.

[4] Q. Han, Y. Xie, J.D. Ordaz, A.J. Huh, N. Huang, W. Wu, N. Liu, K.A. Chamberlain, Z.H. Sheng, X.M. Xu, Restoring cellular energetics promotes axonal regeneration and functional recovery after spinal cord injury, Cell Metabol. 31 (2020) 623–641.

[5] Z. He, Y. Jin, Intrinsic control of axon regeneration, Neuron 90 (2016) 437–451.

[6] A.P. Tran, P.M. Warren, J. Silver, New insights into glial scar formation after spinal cord injury, Cell Tissue Res. (2021) 1–18.

[7] C. Liu, J. Liu, C. Liu, Q. Zhou, Y. Zhou, B. Zhang, Saijilafu, The intrinsic axon regenerative properties of mature neurons after injury, Acta Biochim. Biophys. Sin. 53 (2021) 1–9.

[8] Z.S. Gao, C.J. Zhang, N. Xia, H. Tian, D.Y. Li, J.Q. Lin, X.F. Mei, C. Wu, Berberine-loaded M2 macrophage-derived exosomes for spinal cord injury therapy, Acta Biomater. 126 (2021) 211–223.

[9] X. Liu, M. Hao, Z. Chen, T. Zhang, J. Huang, J. Dai, Z. Zhang, 3D bioprinted neural tissue constructs for spinal cord injury repair, Biomaterials 272 (2021), 120771.

[10] L. Zhang, C. Fan, W. Hao, Y. Zhuang, X. Liu, Y. Zhao, B. Chen, Z. Xiao, Y. Chen, J. Dai, NSCs migration promoted and drug delivered exosomes-collagen scaffold via a bio-specific peptide for one-step spinal cord injury repair, Adv. Healthc. Mater. 10 (2021), 2001896.

[11] K.V. Butler, J. Kalin, C. Brochier, G. Vistoli, B. Langley, A.P. Kozikowski, Rational design and simple chemistry yield a superior, neuroprotective HDAC6 inhibitor, tubastatin A, J. Am. Chem. Soc. 132 (2010) 10842–10846.

[12] Z. Zheng, Y. Zhou, L. Ye, Q. Lu, K. Zhang, J. Zhang, L. Xie, Y. Wu, K. Xu, H. Zhang, J. Xiao, Histone deacetylase 6 inhibition restores autophagic flux to promote functional recovery after spinal cord injury, Exp. Neurol. 324 (2020), 113138.

[13] M.E. Authement, J.N. Kodangattil, S. Gouty, M. Rusnak, S.A. Jymes, B.M. Cox, F.S. Nugent, Histone deacetylase inhibition rescues maternal deprivation-induced GABAergic metaplasticity through restoration of AKAP signaling, Neuron 86 (2015) 1240–1252.

[14] R.D. Shepard, L.D. Langlois, M.E. Authement, F.S. Nugent, Histone deacetylase inhibition reduces ventral tegmental area dopamine neuronal hyperexcitability involving AKAP150 signaling following maternal deprivation in juvenile male rats, J. Neurosci. Res. 98 (2020) 1457–1467.

[15] H. Yang, X. Gao, J. Su, H. Jiang, Y. Lei, W. Ni, Y. Gu, Pharmacokinetics and acute toxicity of a histone deacetylase inhibitor, Scriptaid, and its neuroprotective effects in mice after intracranial hemorrhage, CNS Neurol. Disord. - Drug Targets 19 (2020) 55–65.

[16] H. Yang, X. Gao, J. Su, H. Jiang, Y. Lei, W. Ni, Y. Gu, HDAC inhibition reduces white matter injury after intracerebral hemorrhage, J. Cerebr. Blood Flow Metabol. 41 (2021) 958–974.

[17] C. Hubbert, A. Guardiola, R. Shao, Y. Kawaguchi, A. Ito, A. Nixon, M. Yoshida, X.F. Wang, T.P. Yao, HDAC6 is a microtubule-associated deacetylase, Nature 417 (2002) 455–458.

[18] M.A. Rivieccio, C. Brochier, D.E. Willis, B.A. Walker, M.A. D'Annibale, K. McLaughlin, A. Siddiq, A.P. Kozikowski, S.R. Jaffrey, J.L. Twiss, R.R. Ratan, B. Langley, HDAC6 is a target for protection and regeneration following injury in the nervous system, Proc. Natl. Acad. Sci. USA 106 (2009) 19599–19604.

[19] V. Zwick, C.A. Simões-Pires, A. Nurisso, C. Petit, C.S.P. Dos, G.M. Randazzo, N. Martinet, P. Bertrand, M. Cuendet, Synthesis of a selective HDAC6 inhibitor active in neuroblasts, Bioorg. Med. Chem. Lett 26 (2016) 4955–4959.

[20] S. Shen, M. Svoboda, G. Zhang, M.A. Cavasin, L. Motlova, T.A. McKinsey, J.H. Eubanks, C. Bařinka, A.P. Kozikowski, Structural and in vivo characterization of Tubastatin A, a widely used histone deacetylase 6 inhibitor, ACS Med. Chem. Lett. 11 (2020) 706–712.

[21] J. Xue, J. Xie, W. Liu, Y. Xia, Electrospun nanofibers: new concepts, materials, and applications, Acc. Chem. Res. 50 (2017) 1976–1987.

[22] M. Kharaziha, M. Nikkhah, S.R. Shin, N. Annabi, N. Masoumi, A.K. Gaharwar, G. Camci-Unal, A. Khademhosseini, PGS: gelatin nanofibrous scaffolds with tunable mechanical and structural properties for engineering cardiac tissues, Biomaterials 34 (2013) 6355–6366.

[23] H. Peng, S. Zhou, T. Guo, Y. Li, X. Li, J. Wang, J. Weng, In vitro degradation and release profiles for electrospun polymeric fibers containing paracetanol, Colloids Surf. B Biointerfaces 66 (2008) 206–212.

[24] J. Wang, M. Windbergs, Influence of polymer composition and drug loading procedure on dual drug release from PLGA: PEG electrospun fibers, Eur. J. Pharmaceut. Sci. 124 (2018) 71–79.

[25] R. Hobzova, Z. Hampejsova, T. Cerna, J. Hrabeta, K. Venclikova, J. Jedelska, U. Bakowsky, Z. Bosakova, M. Lhotka, S. Vaculin, M. Franek, M. Steinhart, J. Kovarova, J. Michalek, J. Sirc, Poly (d, l-lactide)/polyethylene glycol micro/ nanofiber mats as paclitaxel-eluting carriers: preparation and characterization of fibers, in vitro drug release, antiangiogenic activity and tumor recurrence prevention, Mater. Sci. Eng. C 98 (2019) 982–993.

[26] E. Dzierzkowska, A. ŚcisŁowska-Czarnecka, S. Matwally, D. Romaniszyn, M. ChadziŃska, E. Stodolak-Zych, Porous poly (lactic acid) based fibres as drug carriers in active dressings, Acta Bioeng. Biomech. 22 (2020) 185–197.

[27] J. Xie, M.R. MacEwan, A.G. Schwartz, Y. Xia, Electrospun nanofibers for neural tissue engineering, Nanoscale 2 (2010) 35–44.

[28] J. Xie, M.R. MacEwan, W. Liu, N. Jesuraj, X. Li, D. Hunter, Y. Xia, Nerve guidance conduits based on double-layered scaffolds of electrospun nanofibers for repairing the peripheral nervous system, ACS Appl. Mater. Interfaces 6 (2014) 9472–9480.

[29] R. Borah, G.C. Ingavle, S.R. Sandeman, A. Kumar, S.V. Mikhalovsky, Amine-functionalized electrically conductive core–sheath MEH-PPV: PCL electrospun nanofibers for enhanced cell–biomaterial interactions, ACS Biomater. Sci. Eng. 4 (2018) 3327–3346.

[30] R. Borah, G.C. Ingavle, S.R. Sandeman, A. Kumar, S.V. Mikhalovsky, Combining electrospun nanofibers with cell-encapsulating hydrogel fibers for neural tissue engineering, J. Biomater. Sci. Polym. Ed. 29 (2018) 1625–1642.

[31] S.H. Lee, B.S. Kim, S.H. Kim, S.W. Choi, S.I. Jeong, I.K. Kwon, S.W. Kang, J. Nikolovski, D.J. Mooney, Y.K. Han, Y.H. Kim, Elastic biodegradable poly (glycolide-co-caprolactone) scaffold for tissue engineering, J. Biomed. Mater. Res. 66 (2003) 29–37.

[32] H. Piao, J.S. Kwon, S. Piao, J.H. Sohn, Y.S. Lee, J.W. Bae, K. Khwang, D.W. Kim, O. Jeon, B.S. Kim, Y.B. Park, M.C. Cho, Effects of cardiac patches engineered with bone marrow-derived mononuclear cells and PGCL scaffolds in a rat myocardial infarction model, Biomaterials 28 (2007) 641–649.

[33] J. Jaworska, R. Smolarczyk, M. Musiał-Kulik, T. Cichoń, P. Karpeta-Jarząbek, J. Włodarczyk, M. Stojko, H. Janeczek, A. Kordyka, B. Kaczmarczyk, M. Pastusiak, J. Kasperczyk, Electrospun paclitaxel delivery system based on PGCL/PLGA in local therapy combined with brachytherapy, Int. J. Pharm. 602 (2021), 120596.

[34] W. Sun, D.A. Gregory, M.A. Tomeh, X. Zhao, Silk fibroin as a functional biomaterial for tissue engineering, Int. J. Mol. Sci. 22 (2021) 1499.

[35] M. Farokhi, F. Mottaghitalab, R.L. Reis, S. Ramakrishna, S.C. Kundu, Functionalized silk fibroin nanofibers as drug carriers: advantages and challenges, J. Contr. Release 321 (2020) 324–347.

[36] Z.N. Hu, S.K. Das, S.Q. Yan, R.C. You, X.F. Li, Z.W. Luo, M.Z. Li, Q. Zhang, D.L. Kaplan, Stability and biodegradation of silk fibroin/hyaluronic acid nerve conduits, Compos. B Eng. 200 (2020), 108222.

[37] R. Brito-Pereira, D.M. Correia, C. Ribeiro, A. Francesko, I. Etxebarria, L. Pérez-Álvarez, J.L. Vilas, P. Martins, S. Lanceros-Mendez, Silk fibroin-magnetic hybrid composite electrospun fibers for tissue engineering applications, Compos. B Eng. 141 (2018) 70–75.

[38] X.G. Huang, X.L. Jiang, Q.Z. Yang, Y.F. Chu, G.Y. Zhang, B. Yang, R.X. Zhuo, Triple-stimuli (pH/thermo/reduction) sensitive copolymers for intracellular drug delivery, J. Mater. Chem. B 1 (2013) 1860–1868.

[39] S. Mura, J. Nicolas, P. Couvreur, Stimuli-responsive nanocarriers for drug delivery, Nat. Mater. 12 (2013) 991–1003.

[40] B. Perrouin-Verbe, C. Lefevre, P. Kieny, R. Gross, B. Reiss, M.F. Le, Spinal cord injury: a multisystem physiological impairment/dysfunction, Rev. Neurol. 177 (2021) 594–605.

[41] L.D. Hachem, M.G. Fehlings, Pathophysiology of spinal cord injury, Neurosurg. Clin. 32 (2021) 305–313.

[42] S. Liu, S.H. Qin, M. He, D.F. Zhou, Q.D. Qin, H. Wang, Current applications of poly (lactic acid) composites in tissue engineering and drug delivery, Compos. B Eng. (2020), 108238.

[43] P. LoPresti, HDAC6 in diseases of cognition and of neurons, Cells 10 (2020) 12.

[44] O. Witt, H.E. Deubzer, T. Milde, I. Oehme, HDAC family: what are the cancer relevant targets? Cancer Lett. 277 (2009) 8–21.

[45] L. Zhang, C. Liu, J. Wu, J.J. Tao, X.L. Sui, Z.G. Yao, Y.F. Xu, L. Huang, H. Zhu, S.L. Sheng, C. Qin, Tubastatin A/ACY-1215 improves cognition in Alzheimer's disease transgenic mice, J. Alzheim. Dis. 41 (2014) 1193–1205.

[46] M.L. Selenica, L. Benner, S.B. Housley, B. Manchec, D.C. Lee, K.R. Nash, J. Kalin, J.A. Bergman, A. Kozikowski, M.N. Gordon, D. Morgan, Histone deacetylase 6 inhibition improves memory and reduces total tau levels in a mouse model of tau deposition, Alzheimer's Res. Ther. 6 (2014) 1–12.

[47] W. Jian, X. Wei, L. Chen, Z. Wang, Y. Sun, S. Zhu, H. Lou, S. Yan, X. Li, J. Zhou, B. Zhang, Inhibition of HDAC6 increases acetylation of peroxiredoxin1/2 and ameliorates 6-OHDA induced dopaminergic injury, Neurosci. Lett. 658 (2017) 114–120.

[48] Z. Wang, Y. Leng, J. Wang, H.M. Liao, J. Bergman, P. Leeds, A. Kozikowski, D.M. Chuang, Tubastatin A, an HDAC6 inhibitor, alleviates stroke-induced brain infarction and functional deficits: potential roles of α-tubulin acetylation and FGF-21 up-regulation, Sci. Rep. 6 (2016), 19626.

[49] Y. Yao, J. Xu, T. Yu, Z. Chen, Z. Xiao, J. Wang, Y. Hu, Y. Wu, D. Zhu, Flufenamic acid inhibits secondary hemorrhage and BSCB disruption after spinal cord injury, Theranostics 8 (2018) 4181–4198.

[50] A.L. Kalinski, A.N. Kar, J. Craver, A.P. Tosolini, J.N. Sleigh, S.J. Lee, A. Hawthorne, P. Brito-Vargas, S. Miller-Randolph, R. Passino, L. Shi, V.S.C. Wong, C. Picci, D.S. Smith, D.E. Willis, L.A. Havton, G. Schiavo, R.J. Giger, B. Langley, J.L. Twiss, Deacetylation of Miro1 by HDAC6 blocks mitochondrial transport and mediates axon growth inhibition, JCB (J. Cell Biol.) 218 (2019) 1871–1890.